Proceedings of IMECE 2000:
International Mechanical Engineering Congress & Exposition
November 5-10, 2000
Walt Disney World Dolphin
Orlando, Florida

GEOMETRICAL NON-LINEAR PERIODIC VIBRATION OF PLATES

M. Petyt
Institute of Sound and Vibration Research, University of Southampton,
Southampton SO17 1BJ, England

P. Ribeiro
DEMEGI, Faculdade de Engenharia, Universidade do Porto,
Rua dos Bragas, 4050-123 Porto, Portugal

ABSTRACT

Periodic, geometrically non-linear free and steady-state forced vibrations of fully clamped plates are investigated. The hierarchical finite element method (HFEM) and the harmonic balance method are used to derive the equations of motion in the frequency domain, which are solved by a continuation method. It is demonstrated that the HFEM requires far fewer degrees of freedom than the *h*-version of the FEM. Internal resonances due to modal coupling between modes with resonance frequencies related by a rational number, are discovered. In free vibration, internal resonances cause a very significant variation of the mode shape during the period of vibration. A similar behaviour is observed in steady-state forced vibration. The stability of the steady-state solutions is studied by Floquet's theory and it is shown that stable multi-modal solutions occur.

1 INTRODUCTION

When subjected to large dynamic excitations or to excitations with a frequency component close to a natural frequency, thin plates can undergo large amplitude, geometrical non-linear vibrations. This occurs typically with aircraft skin-panels, due to high levels of aerodynamic forces and acoustic pressure.

In plates with fixed edges, geometric non-linearity causes an increase of the resonance frequencies and a variation of the non-linear mode shapes with the amplitude of vibration (Benamar et al., 1994; Han, 1993; Han and Petyt, 1997a, b). Because they change with amplitude, the natural frequencies may easily become commensurable, that is related by $m_1\omega_1+m_2\omega_2+ \ldots + m_n\omega_n \cong 0$, where m_i are integers. As a consequence, the normal modes may couple, and multi-frequency, multi-modal response occur. This phenomenon is known as internal resonance (Szemplinska-Stupnicka, 1990).

The *h*-version of the FEM, where the mesh is refined in order to achieve convergence, leads to an accurate spatial model and allows one to describe the variation of the mode shape of the plate with the amplitude of vibration displacement. It has been used, for example, by Lau et al. (1984a, b), Mei and Decha-Umphai (1985) and Rao et al. (1993). The FEM non-linear equations are solved by iterative methods, with a recalculation of the non-linear matrices in each iteration. Therefore, the number of degrees of freedom (d.o.f.) has a substantial influence on the time needed to solve the model. In geometrical non-linear vibrations turning and bifurcation points may exist, leading to regions with multiple solutions. Continuation methods (Seydel, 1988) are able to pass turning points, to discover bifurcation points and, in most cases, to follow secondary branches. However, these methods are computationally heavier than other simpler methods of solving the equations of motion, increasing the importance of having an accurate model with a reduced number of d.o.f.

Plates vibrating with displacement amplitudes of the order of their thickness, either in free vibration or due to harmonic excitation, usually experience periodic motion and, consequently, the harmonic balance method (HBM) can be applied (Ribeiro, 1998). This method relies upon assuming a time solution in the form of a Fourier series, reducing the problem to that of solving a system of non-linear differential equations in the space variables. It is not restricted to weakly non-linear systems, is simple, has a clear physical meaning and is easy to implement computationally. However, it may be necessary to use several harmonics in the Fourier series, increasing the number of degrees of freedom. This is one more reason why it is important to have a spatial model with a small number of d.o.f.

In the *p*-version of the FEM, the accuracy of the approximation is improved by increasing the number of shape functions over the elements. If the set of functions corresponding to an approximation of lower order p, constitutes a subset of the set of functions corresponding to the approximation of order p+1, then the *p*-version of the FEM is called the "hierarchical finite element method" (HFEM).

Han and Petyt (1993, 1997a, b) studied harmonic free vibrations of isotropic and laminated plates with geometrical non-linearity by the HFEM. This method was used in conjunction with a continuation method to investigate free and steady-state harmonic vibrations of isotropic and composite plates by Ribeiro and Petyt (1999a, b). Ribeiro and Petyt (1999c-e, 2000) also studied internal resonances, and multi-modal, multi-frequency free and steady-state forced vibrations of isotropic and laminated plates by the HFEM and the HBM, using more then one term in the Fourier series. It was shown that internal resonances result in an important change of the plates' non-linear mode shape, with consequences in free and forced vibration. They may also result in a secondary branch of the backbone curve or in "complex" curvatures of a main branch of this curve or of the frequency response curve. The backbone curve relates the frequency with the amplitude of vibration in free vibration and a main branch of this curve is one that originates from a linear solution. The designation FRF is applied to steady-state forced vibration by similarity with linear analysis, in spite of the fact that in non-linear analysis the "FRF" depends on the amplitude of excitation. The works referred to demonstrate that, because high-order polynomial displacement shape functions are used in the HFEM only one element is needed to model the whole plate, and the model has far fewer d.o.f. than in the *h*-version of the finite element method.

In this paper, which is essentially an abridged version of Ribeiro and Petyt (1999a, d, e and 2000), the hierarchical finite element method is used to construct the geometrical non-linear spatial model of thin, rectangular, isotropic plates. The harmonic balance method is applied to derive the equations of motion in the frequency domain, which are solved by a continuation method. Free vibrations and the response of the plates to external harmonic excitations are analysed. The convergence of the solution with the number of harmonics and with the number of shape functions is investigated. Fully clamped boundaries are considered because they are adequate to model many real panel-type situations, such as aircraft wing panels. However, the methods presented can be applied to plates with any boundary conditions. The stability of the solutions is determined applying Floquet's theory and the internal resonance phenomenon is investigated.

2 EQUATIONS OF MOTION

2.1 Hierarchical Finite Element Model

The middle plane displacements u_0, v_0 and w_0 of each element - Fig. 1 - are expressed in the form:

$$\begin{Bmatrix} u_0 \\ v_0 \\ w_0 \end{Bmatrix} = [N] \begin{Bmatrix} q_p \\ q_w \end{Bmatrix} \tag{1}$$

where

$$[N] = \begin{bmatrix} \lfloor N^u \rfloor & 0 & 0 \\ 0 & \lfloor N^u \rfloor & 0 \\ 0 & 0 & \lfloor N^w \rfloor \end{bmatrix} \tag{2}$$

$$\lfloor N^u \rfloor = \lfloor g_1(\xi) g_1(\eta) \;\; g_1(\xi) g_2(\eta) \cdots g_{p_i}(\xi) g_{p_i}(\eta) \rfloor \tag{3}$$

$$\lfloor N^w \rfloor = \lfloor f_1(\xi) f_1(\eta) \;\; f_1(\xi) f_2(\eta) \cdots f_{p_o}(\xi) f_{p_o}(\eta) \rfloor \tag{4}$$

and p_i and p_o are the number of in-plane and out-of-plane shape functions used in the model; $\{g\}$ and $\{f\}$ are the vectors of in- and out-of-plane shape functions; $\{q_p\}$ and $\{q_w\}$ are the generalised in- and out-of-plane displacements and $[N]$ the matrix of shape functions. The shape functions used are the Rodrigues' form of Legendre polynomials (Ribeiro and Petyt, 1999a), which satisfy fully clamped boundary conditions. To study plates with different boundary conditions or if more than one element is necessary, other shape functions - for example the third order polynomials commonly used in the *h*-version of the FEM - are added.

For smooth solutions the introduction of higher order shape functions gives greater accuracy than a refinement of the mesh. Therefore, the whole plate is modeled with one element only and the relation between the local and global co-ordinates is

$$\xi = 2x/a, \;\; \eta = 2y/b \tag{5}$$

Only thin plates are analysed, thus the transverse shear and rotatory inertia can be neglected (Chia, 1980). The geometrical non-linearity is expressed by the non-linear strain-displacement relationships of von Kármán, which are given by

$$\begin{Bmatrix} \varepsilon_x \\ \varepsilon_y \\ \gamma_{xy} \end{Bmatrix} = \begin{bmatrix} 1 & 0 & 0 & z & 0 & 0 \\ 0 & 1 & 0 & 0 & z & 0 \\ 0 & 0 & 1 & 0 & 0 & z \end{bmatrix} \{\varepsilon\} = [[I] \quad z[I]] \{\varepsilon\} \tag{6}$$

where

$$\{\varepsilon\} = \begin{Bmatrix} \varepsilon_o^p \\ \varepsilon_o^b \end{Bmatrix} + \begin{Bmatrix} \varepsilon_L^p \\ 0 \end{Bmatrix} \tag{7}$$

$\{\varepsilon_0^p\}$ and $\{\varepsilon_0^b\}$ are the linear membrane and bending strains; $\{\varepsilon_L^p\}$ is the geometrically non-linear membrane strain. They are defined as

$$\{\varepsilon_o^p\} = \begin{Bmatrix} u_{,x} \\ v_{,y} \\ u_{,y} + v_{,x} \end{Bmatrix}, \; \{\varepsilon_o^b\} = \begin{Bmatrix} -w_{,xx} \\ -w_{,yy} \\ -2w_{,xy} \end{Bmatrix}, \; \{\varepsilon_L^p\} = \begin{Bmatrix} (w_{,x})^2/2 \\ (w_{,y})^2/2 \\ w_{,x} w_{,y} \end{Bmatrix} \tag{8}$$

where $,x$ denotes differentiation with respect to x.

The equations of motion are derived by equating the sum of the virtual work of the inertia forces, of the elastic restoring forces and of the external forces to zero. The external forces are applied only in the transverse direction. In isotropic plates, there is no coupling between in-plane stretching and transverse bending. Thus, applying the principle of the virtual work one obtains:

$$\int_\Omega \left(\{\delta\varepsilon_o^p\}^T + \{\delta\varepsilon_L^p\}^T \right) [A] \left(\{\varepsilon_o^p\} + \{\varepsilon_L^p\} \right) d\Omega + \int_\Omega \{\delta\varepsilon_o^b\}^T [D] \{\varepsilon_o^b\} d\Omega +$$

$$\int_\Omega \rho h \left(\delta u_0 \ddot{u}_0 + \delta v_0 \ddot{v}_0 + \delta w_0 \ddot{w}_0 \right) d\Omega = \lfloor \delta u \quad \delta v \quad \delta w \rfloor \int_\Omega [N]^T \begin{Bmatrix} 0 \\ 0 \\ \overline{P}_d(x,y,t) \end{Bmatrix} \tag{9}$$

where ρ denotes the mass density; $\overline{P}_d(x,y,t)$ is the distributed applied force (N/m^2) and Ω is the area of the plate. [*A*] and [*D*] are the membrane and flexural rigidity matrices given by

$$[A]=\frac{Eh}{(1-\nu^2)}\begin{bmatrix}1 & \nu & 0\\ \nu & 1 & 0\\ 0 & 0 & \frac{1}{2}(1-\nu)\end{bmatrix} \quad \text{and} \quad [D]=\frac{h^2}{12}[A] \qquad (10, 11)$$

where E is Young's modulus, ν Poisson's ratio and h the plate thickness.

Substituting Eqs. (8) into Eq. (9) and allowing the virtual generalised displacements to be arbitrary gives:

$$\begin{bmatrix}M_p & 0\\ 0 & M_b\end{bmatrix}\begin{Bmatrix}\ddot{q}_p\\ \ddot{q}_w\end{Bmatrix}+\left(\begin{bmatrix}K_{1p} & 0\\ 0 & K_{1b}\end{bmatrix}+\begin{bmatrix}0 & K_2\\ 0 & 0\end{bmatrix}+\begin{bmatrix}0 & 0\\ K_3 & 0\end{bmatrix}+\begin{bmatrix}0 & 0\\ 0 & K_4\end{bmatrix}\right)\begin{Bmatrix}q_p\\ q_w\end{Bmatrix}=\begin{Bmatrix}0\\ \overline{P}\end{Bmatrix} \qquad (12)$$

$[M_p]$ and $[M_b]$ are the in-plane and bending inertia matrices; $[K_{1p}]$ and $[K_{1b}]$ the in-plane and bending linear stiffness matrices; $[K_2]$, $[K_3]$ and $[K_4]$ the non-linear stiffness matrices and $\{\overline{P}\}$ is the vector of generalised external forces. $[K_2]$ and $[K_3]$ depend linearly on $\{q_w\}$, $[K_4]$ depends quadratically on $\{q_w\}$. All sub-matrices in Eq. (12) are symmetric except $[K_2]$ and $[K_3]$, which are related by $[K_3]=2[K_2]^T$ (Han, 1993).

Neglecting the middle plane in-plane inertia, and thus eliminating the in-plane generalised displacements, and introducing mass proportional hysteretic damping (Ribeiro, 1998), the following equations of motion are obtained

$$[M_b]\{\ddot{q}_w\}+\frac{\beta}{\omega}[M_b]\{\dot{q}_w\}+[K_{1b}]\{q_w\}+[Knl]\{q_w\}=\{\overline{P}\} \qquad (13)$$

where $[Knl]=[K_4]-2[K_2]^T[K_{1p}]^{-1}[K_2]$ is a quadratic function of the transverse generalised displacements, $\{q_w\}$. The non-linearity is thus of the cubic type and the system of Eqs. (13) is a system of Duffing equations. The damping factor β is given by

$$\beta=\alpha\omega_{\ell 1}^2 \qquad (14)$$

where $\omega_{\ell 1}$ is the first linear natural frequency.

2.2 Harmonic Balance Method

The excitations considered are of the form $\{\overline{P}\}=\{P\}\cos(\omega t)$ and only periodic motions are analysed. Thus, the steady state response $\{q_w(t)\}$ can be written as:

$$\{q_w(t)\}=\sum_{i=1,3,\ldots}^{2k-1}\{w_{ci}\}\cos(i\omega t)+\{w_{si}\}\sin(i\omega t) \qquad (15)$$

and the harmonic balance method applied. Because the non-linearity is cubic and the excitation harmonic, only odd harmonics are taken into account (Ribeiro, 2000). Equation (15) is inserted into the equations of motion (13) and the coefficients of the same harmonic components are compared. The ensuing equations of motion in the frequency domain are of the form:

$$\{F\}=\left(-\omega^2[M]+[C]+[KL]+[KNL]\right)\{w\}-\{P\}=\{0\} \qquad (16)$$

In Eqs. (16), $[M]$ represents the mass matrix, $[C]$ represents the damping matrix and $[KL]$ represents the linear stiffness matrix. These matrices are constant. $[KNL]$ represents the non-linear stiffness matrix, which is formed by a combination of $[K_4]$ and $[K_2]$ and depends quadratically on the vector of generalised displacements $\{w\}^T=\lfloor w_{c1}\ \ w_{s1}\ \ w_{c3}\ \ w_{s3}\ \ \ldots\ \ w_{ci}\ \ w_{si}\rfloor$. All the matrices in Eq. (16) depend on the number of harmonics chosen. They are explicitly given in Ribeiro and Petyt (1999a, c and 2000) for undamped and damped systems, employing different numbers of harmonics.

The high order integrals involved in calculating the matrices in Eq. (16) are accurately evaluated using symbolic computation, which is also helpful in the application of the harmonic balance method. The total number of degrees of freedom of the model, n, is given by $n=2kp_o^2$, for a damped model, or $n=kp_o^2$, for an undamped model, where k represents the number of harmonics.

3 SOLUTION OF THE EQUATIONS OF MOTION

Several iterative methods can be applied to solve the equations of motion. The simplest may be named *linearized updated mode* (LUM), after Chiang et al. (1991). This method consists on the consecutive solution of an eigenvalue problem and has in its simplicity the greatest advantage. Another option is to use the well-known Newton method, which has greater rates of convergence then the LUM method, but requires the calculation of a Jacobian matrix. None of these methods is capable of passing turning points and of describing secondary branches characteristic of non-linear systems, and, therefore, a continuation method (Lewandowski, 1994; Ribeiro and Petyt, 1999a; Seydel, 1988) based on the Newton method and a constraint equation, is applied in this paper.

The continuation method is composed of two main loops: one external and one internal. In the external loop, a predictor to the solution is defined, using the two last determined points of the backbone curve in free vibration and of the FRF in forced vibration. In the internal loop, the approximated solution is corrected by applying Newton method to Eq. (16), considering variations not only in the generalised co-ordinates but also in the frequency of vibration. Thus, the following equation is solved:

$$[J]\{\delta w\}-[M]\{w\}\,\delta\omega^2=-\{F\} \qquad (17)$$

where $\{F\}$ is defined by Eq. (16) using the last vector of generalised displacements; $\{\delta w\}$ and $\delta\omega^2$ represent, respectively, the corrections of the vector of generalised displacements and of the square of the frequency of vibration.

In Eq. (17) there are n variables and $n+1$ unknowns. Another equation is defined by constraining the arc-length s, that is the distance between two successive points of the curve, to a fixed value:

$$s^2=\|\Delta\{w\}\|^2=Const. \qquad (18)$$

The iterations are repeated until the following inequalities are satisfied:

$$\left|\delta\omega^2/\omega^2\right|<error1,\ \ \|\{\delta w\}\|/\|\{w\}\|<error2,\ \ \|\{F\}\|<error3 \qquad (19, 20, 21)$$

Matrix $[J]$ in Eq. (17) is the Jacobian matrix, defined as

$$[J]=\partial\{F\}/\partial\{w\} \qquad (22)$$

For systems with a small number of degrees of freedom, the former matrix may be computed exactly using symbolic computation. Otherwise, the following approximation may be used:

$$[J] \cong -\omega^2[M]+[C]+[KL]+3[KNL] \tag{23}$$

This expression was derived by applying variations to Eq. (16) (Ribeiro and Petyt, 1999a). As the error criteria must be fulfilled, the solution obtained with an approximated Jacobian is still accurate. It is important to verify if the equilibrium equations are satisfied, as expressed in Eq. (21). If the middle-plane in-plane displacements are not included in the model, $[K_2]$ does not exist and the former approximation is exact.

If the signs of the determinant of the Jacobian matrix, $|J|$, of two successive points of the backbone curve are different, then there exists a particular point between those two points for which $|J|=0$ and the matrix $[J]$ is singular. A solution $\left(\{w\}_0, \omega_0^2\right)$ of $\{F\}=\{0\}$, for which the Jacobian matrix is singular is an exceptional point, i.e., it is a bifurcation or a turning point (Seydel, 1988). From bifurcation points, secondary branches are born. In order to describe secondary branches, a point close to the bifurcation point is used to calculate the Jacobian matrix and the eigenvalue problem

$$([J]-\mu[I])\{\phi\} = \{0\} \tag{24}$$

is solved. The eigenvector(s) $\{\phi_j\}$ associated with the zero eigenvalue(s) $\mu_j=0$ indicate the direction(s) to be followed. The perturbed configuration, $\{w\}_j$, which is used as starting vector for branch switching, is obtained by adding the scaled eigenvector to the solution vector $\{w\}$ at the point close to the bifurcation:

$$\{w\}_j = \{w\} + \zeta_j \frac{\{\phi_j\}}{\|\{\phi_j\}\|} \tag{25}$$

where ζ_j denotes a scaling factor.

4 STABILITY OF THE SOLUTIONS

In a non-linear system several equilibrium solution may be obtained, but only stable equilibrium solutions exist actually and are physically meaningful (Szemplinska-Stupnicka, 1990). The study of the stability of the equilibrium solutions is therefore of great importance. This can be carried out by adding a small disturbance to the steady state solution

$$\{\tilde{q}\} = \{q_w\} + \{\delta q_w\} \tag{26}$$

and analysing the evolution of $\{\delta q_w\}$. If $\{\delta q_w\}$ dies out with time then $\{q_w\}$ is stable, if it grows then $\{q_w\}$ is unstable.

Inserting the disturbed solution (26) into Eq. (13), expanding the non-linear terms by means of Taylor series around $\{q_w\}$ and ignoring terms of order higher than $\{\delta q_w\}$, the following equations are obtained:

$$[M_b]\{\delta\ddot{q}_w\}+\frac{\beta}{\omega}[M_b]\{\delta\dot{q}_w\}+[K1_b]\{\delta q_w\}+\frac{\partial([Knl]\{q_w\})}{\partial\{q_w\}}\{\delta q_w\}=\{0\} \tag{27}$$

The coefficients $\partial([Knl]\{q_w\})/\partial\{q_w\}$ are periodic functions of time and can be expanded in a Fourier series:

$$\frac{\partial([Knl]\{q_w\})}{\partial\{q_w\}} = [p_1]+[p_2]\cos(2\omega t)+[p_3]\sin(2\omega t)+[p_4]\cos(4\omega t) + [p_5]\sin(4\omega t)+h.o.t. \tag{28}$$

where *h.o.t.* stands for higher order terms, which will be neglected. The Fourier coefficients of $\partial([Knl]\{q_w\})/\partial\{q_w\}$ - $[p_1]$, $[p_2]$, $[p_3]$, $[p_4]$ and $[p_5]$ - are quadratic functions of $\{q_w\}$ and can be written in the form

$$[p_1]=\frac{1}{T}\int_0^T \frac{\partial}{\partial q_w}([Knl]\{q_w\})dt \tag{29}$$

$$[p_{2i}]=\frac{2}{T}\int_0^T \frac{\partial}{\partial q_w}([Knl]\{q_w\})\cos(2i\omega t)dt,\ i=1,2 \tag{30}$$

$$[p_{2i+1}]=\frac{2}{T}\int_0^T \frac{\partial}{\partial q_w}([Knl]\{q_w\})\sin(2i\omega t)dt,\ i=1,2 \tag{31}$$

Inserting Eq. (28) into Eq. (27), results in

$$[M_b]\{\delta\ddot{q}_w\}+\frac{\beta}{\omega}[M_b]\{\delta\dot{q}_w\}+[K_{1b}]\{\delta q_w\}+[[p_1]+[p_2]\cos(2\omega t) + [p_3]\sin(2\omega t)+[p_4]\cos(4\omega t)+[p_5]\sin(4\omega t)]\{\delta q_w\}=\{0\} \tag{32}$$

which forms a system of Hill's equations (Szemplinska-Stupnicka, 1990).

The modal co-ordinates , $\{\delta\xi\}$,of the linear system are defined by

$$\{\delta q_w\} = [B]\{\delta\xi\} \tag{33}$$

where $[B]$ represents the modal matrix. The modal co-ordinates are normalised so that the matrix of modal masses is the identity matrix. Using modal co-ordinates, multiplying Eq. (32) by $[B]^T$ and introducing a new vector of variables defined as

$$\{\delta\xi\} = e^{-\frac{1}{2}\frac{\beta}{\omega}[I]t}\{\delta\bar{\xi}\} \tag{34}$$

the following system of equations is obtained:

$$\{\delta\ddot{\bar{\xi}}\}+\left([\omega_j^2]-\frac{1}{4}\left(\frac{\beta}{\omega}\right)^2[I]+[B]^T([p_1]+[p_2]\cos(2\omega t)+ [p_3]\sin(2\omega t)+[p_4]\cos(4\omega t)+[p_5]\sin(4\omega t))[B]\right)\{\delta\bar{\xi}\}=\{0\} \tag{35}$$

The simplification to Eq. (35) was only possible because, after transformation into modal co-ordinates, the damping matrix is non-singular, and is equal to a scalar times the identity matrix and therefore commutes with any other matrix.

The solution of (35) is assumed to have the form

$$\{\delta\bar{\xi}\}=e^{\lambda t}(\{b_1\}\cos(\omega t)+\{a_1\}\sin(\omega t)+\{b_3\}\cos(3\omega t)+\{a_3\}\sin(3\omega t)) \tag{36}$$

where λ are the characteristic exponents. With this expression, simple instabilities of first and of third order are detected. Inserting (36) into (35) and applying the HBM one arrives at the following system of equations:

$$\left(\lambda^2[I]+\lambda[M_1]+[M_0]\right)\{X\}=\{0\} \tag{37}$$

where $[I]$ is the identity matrix and $\{X\}^T=\lfloor b_1 \quad a_1 \quad b_3 \quad a_3 \rfloor^T$. Defining $\{\Gamma\}=\lambda\{X\}$, the following eigenvalue problem is derived

$$\begin{bmatrix} 0 & [I] \\ -[M_0] & -[M_1] \end{bmatrix}\begin{Bmatrix} X \\ \Gamma \end{Bmatrix}=\lambda\begin{Bmatrix} X \\ \Gamma \end{Bmatrix} \tag{38}$$

The characteristic exponents λ are the eigenvalues of the double size matrix in Eq. (38). If the real part of $\lambda-\beta/(2\omega)$ is positive for any λ, then the solution is unstable, otherwise it is stable. Only the eigenvalues with major real part must be determined, however, for systems with a large number of d.o.f., this may take a long time. A simplification of the stability study, is possible by using the sign of $|J|$ (Ribeiro and Petyt, 1999e), which is needed in the continuation method. In this simplified approach, the characteristic exponents are only calculated for the first point of the curve and when there is an indication that $|J|$ was zero. However, in this way higher order losses of stability are not detected.

5 NUMERICAL APPLICATIONS

Two steel plates and an aluminium plate are studied. Their geometrical and material properties are given in Tables 1 and 2. In investigations of geometrical non-linear vibrations by the FEM, it is usually considered that the vibration is harmonic. Thus in a first subsection, only harmonic vibration is studied and results are compared with published results. In this way the HFEM model is validated and it is demonstrated that it requires a small number of d.o.f. In a second sub-section more harmonics are considered in the Fourier series and multi-modal vibration is studied. All edges of the plates are clamped and immovable.

Table 1 Geometric properties

Plate	*a* (mm)	*b* (mm)	*h* (mm)
1	486	322.9	1.2
2	500	500	2.0833
3	300	320	1

Table 2 Material properties

Plate	Material	E (N/m^2)	ρ (Kg/m^3)	ν
1 and 2	steel	21.0×10^{10}	7800	0.3
3	aluminium	7×10^{10}	2778	0.34

5.1 Harmonic vibration

In this sub-section Plates 1 and 2 are analysed. First, the convergence of the solutions with the number of shape functions is investigated, in free vibrations and in forced vibrations due to a harmonic plane wave at normal incidence. Since the plates, the external excitation and the boundary conditions are symmetric with respect to both axes *x* and *y*, only modes for which the transverse displacement is symmetric with respect to *x* and *y* (doubly-symmetric) are excited. Thus, only symmetric out-of-plane shape functions need to be included in the model. However, both symmetric and antisymmetric in-plane shape functions must be used. In fact, the in-plane displacement components are anti-symmetric with respect to one axis and symmetric with respect to the other, that is: $u(x,y)=u(x,-y)=-u(-x,y)$ and $v(x,y)=v(-x,y)=-v(x,-y)$.

In Table 3 the convergence of the linear natural frequency values of Plate 1 with the number of out-of-plane shape functions is shown. The mode numbers (n_1, n_2) are related to the modal lines: n_1 and n_2 are one plus the number of nodal lines crossing any line parallel to the *x*-axis and *y*-axis, respectively. The plate edges are not counted. In Fig. 2 the backbone curves and the frequency response function (FRF) curves are displayed for different values of p_o and for p_i = 6. The amplitude of the external force is 10 N/m^2 and w_{max} represents the amplitude of vibration displacement. Both in the linear and in the non-linear cases, the results obtained with p_o = 2 are accurate around mode (1,1). For the modes (1,3) and (1,5), three out-of-plane shape functions provide a very reasonable approximation to the solution. This means that with 9 d.o.f. in undamped vibration, and 18 d.o.f. if damping is included, the first three modes can be analysed.

Table 3 Linear natural frequencies(rad/s) of Plate 1

p_o	2	3	4	5
Mode (1,1)	487.343	487.283	487.276	487.276
Mode (1,3)	1233.04	1197.30	1195.92	1195.91
Mode (1,5)	2378.31	2267.64	2263.73	2263.69

A study of the convergence with p_i was also carried out (Ribeiro and Petyt, 1999a). For the amplitudes studied, p_i=4 provides results with a good accuracy. The influence of the middle plane in-plane displacements is particularly important for larger amplitudes of vibration, and their exclusion (p_i=0) increases the stiffness of the model. The rate of convergence with p_o and p_i is the same in free and forced vibration. The value of p_i affects more the non-linear behavior than the value of p_o, because the non-linearity is related with the action of the membrane forces.

In Fig. 3 the first resonance frequencies of Plate 1, obtained with the HFEM, are compared with the experimental ones (Benamar et al., 1994). The agreement is quite good. Due to the finite stiffness of any clamping structure, exact clamped conditions are not possible in practice. This possibly explains most of the difference between the HFEM and the experimental values.

For Plate 2, comparison is made in Table 4 between the frequency ratios calculated in this paper and published ones. Because the amplitude is not a parameter in the continuation method, the values of w_{max}/h are not multiples of 0.1. The number of d.o.f. is much lower in the HFEM model than in the *h*-version finite element method used by Rao et al. (1993). The results in this paper agree closely with the ones of Han and Petyt (1997), in which the HFEM was also applied, but the equations of motion were solved by the LUM method. The symmetries of the problem were used in the present work, substantially reducing the number of d.o.f.

The FRF curves of Plate 1 excited by plane waves at normal incidence and at grazing, or tangential, incidence along the *x*-axis (Ribeiro and Petyt, 1999a) are displayed in Figs. 4 and 5 For similar excitation amplitudes, P=10 N/m^2, the maximum amplitudes of vibration caused by the two different excitations occur around the first mode and are similar – Figs. 4 a) and 5 a). However, the wave at grazing incidence excites modes that are not doubly-symmetric, explaining the second resonance in Fig. 5 b), at $\omega/\omega_{\ell 1}\cong 1.54$. Therefore, both symmetric and anti-symmetric shape functions must be used with this type of excitation.

Table 4 Frequency ratios $\omega/\omega_{\ell 1}$ of fully clamped square plates

$\frac{w_{\max}}{h}$	$\omega/\omega_{\ell 1}$, 49 d.o.f.†	$\omega/\omega_{\ell 1}$, 36 elements, 40 d.o.f. each‡	HF EM 9 d.o.f. (p_o=3, p_i=6)	
			$w_{\max}/h$	$\omega/\omega_{\ell 1}$
0.2	1.0068	1.0095	0.2099	1.0079
0.6	1.0600	1.0825	0.6007	1.0632
1	1.1599	1.2149	1.0011	1.1670

† Han and Petyt, 1997a; ‡ Rao et al., 1993.

With the continuation method, stable and unstable solutions were obtained, as shown in Figs. 4 and 5. The solutions' simple stability of first order was studied by using the sign of the determinant as an indicator of change in adjacent solution's stability status. This approach was confirmed by a complete determination of the characteristic exponents, which is not very time demanding when using the present model, due to its small number of d.o.f.

The frequency ratios of Plate 2, when this one is subjected to an uniform harmonic distributed force of amplitude P_d=873.82 N/m^2 are shown in Table 5. Nine d.o.f. are sufficient to achieve convergence and the values calculated are, with the exception of the one at $w_{\max}/h$ = +0.2, close to the values calculated by Mei and Decha-Umphai (1985) using the *h*-version of the FEM with many more d.o.f.

5.2 Multi-harmonic vibration

In this subsection, the aluminium plate, Plate 3, is studied. It is intended to demonstrate that an accurate model of multi-harmonic vibration can be constructed with a small number of d.o.f. Therefore, the convergence with the number of harmonics and with the number of shape functions is discussed first. Internal resonances and the effect they have on the dynamic behaviour of the plate are studied afterwards. Only free and forced vibrations in the vicinity of the first mode are studied, but the methods can be applied to higher order modes.

In Plate 3, modes four and higher can interact with the first one due to 1:3 internal resonances, because $\omega_{\ell 4}/\omega_{\ell 1}$ >3. Therefore, the backbone curves were calculated at points (ξ,η)=(0,0) where the largest amplitude of vibration of the first mode is achieved, and (ξ,η)=(0.5,0.5), where mode 4 has a large vibration amplitude. In order to avoid the inclusion of too many figures, only some of the curves will be shown. The linear mode shapes and natural frequencies of Plate 3 are represented in Ribeiro and Petyt (2000).

Figure 6 demonstrates that the one harmonic approximation is only accurate for amplitudes of vibration lower than 0.8*h* at point (ξ,η)= (0,0). In this and the following figures, w_m represents the maximum amplitude of vibration displacement attained during the cycle, at the points (ξ, η) indicated, and is given by

$$w_m = \lfloor N_w \rfloor \sum_{i=1,3}^{2k-1} \{w_i\} \tag{39}$$

where *k* represents the number of harmonics. For amplitudes of the order of the plate's thickness, the two harmonics approximation is very accurate. Consequently, two harmonics will be used in the following analysis. In all the backbone curves, the frequency ω of the *x* axis is the frequency of vibration of the first harmonic (the third harmonic actually has a frequency 3ω and the fifth 5ω).

Table 5 Relation between the frequency ratio $\omega/\omega_{\ell 1}$ and the amplitude of vibration $w_{\max}/h$ in a square plate subjected to harmonic distributed force P_0=0.2*

$\frac{w_{\max}}{h}$	*9 elements, 24 d.o.f. each. $\omega/\omega_{\ell 1}$	HFEM p_o=3, p_i=6 (9 d.o.f.)	
		$w_{\max}/h$	$\omega/\omega_{\ell 1}$
±0.2	0.1180	+.2001	0.2442
	1.4195	-.2005	1.4399
±0.6	0.8905	+.5992	0.8962
	1.2083	-.5997	1.2114
±1	1.0700	+1.000	1.0800
	1.2429	-1.001	1.2491

* From Mei and Decha-Umphai (1985): $P_0 = cP_d/\rho h^2\omega_1^2$ $c = \iint \phi dxdy / \iint \phi^2 dxdy$, ϕ - normalized mode shape. P_d - amplitude of external force (N/m^2).

Regarding the linear natural frequencies, five out-of-plane shape functions (25 d.o.f.) give a very good approximation to the first eight linear natural frequencies and with seven out-of-plane shape functions (49 d.o.f.) the first ten linear frequencies are accurately calculated. The backbone curve of the plate's first and third harmonics are accurately calculated with p_o=5, the first harmonic is accurately calculated with seven in-plane shape functions and the third harmonic requires, for the frequency regions considered, at least eight in-plane shape functions (Ribeiro and Petyt, 2000). The number of in-plane shape functions necessary increases with the amplitude of vibration, because the middle plane in-plane displacements become more important.

It should be pointed out that in multi-harmonic vibration, symmetric modes can excite anti-symmetric ones. Therefore, no assumption regarding the spatial symmetry of the solutions was adopted: both symmetric and anti-symmetric out-of-plane and in-plane shape functions are always used in this section.

In Fig. 7 the branch diagrams of the plate at (ξ,η)=(0.5,0.5) are shown. The amplitude of the i^{th} harmonic is given by:

$$W_i = \sqrt{\left(\lfloor N_w \rfloor w_{ci}\right)^2 + \left(\lfloor N_w \rfloor w_{si}\right)^2} \tag{40}$$

where the out-of-plane shape functions are calculated at the coordinates (ξ,η) indicated. In undamped systems, w_{si}=0.

There are two main branches linked by a secondary branch, between two bifurcation points. Let us first concentrate upon frequencies of vibration $\omega/\omega_{\ell 1}$<1.1. The first main branch is born from the first linear mode and for those frequencies it is mainly defined by the first harmonic. Although the mode shapes associated with points of the first main branch change with the amplitude of vibration displacement, they are similar to the first linear mode shape, mode (1,1). The second main branch is related with the fourth mode of vibration, mode (2,2), and with the third harmonic. The mode shape changes with the amplitude of vibration displacement, but is similar to the fourth linear mode shape.

The first and fourth linear natural frequencies are related by $\omega_{\ell 4}/\omega_{\ell 1}$=3.0057 and when $\omega_{n\ell 1}$ increases a 1:3 internal resonance and a bifurcation point occur. The first mode, which is axisymmetric with respect to the *z*-axis, and the fourth mode, which is anti-symmetric with respect to both planes *x*-*z* and *y*-*z*, couple. A secondary branch is born in the bifurcation point of the first main branch and finishes at a bifurcation point in a second main branch. As one moves along the secondary branch, from the first main branch to the second main branch, the importance of the first harmonic decreases while the importance of the second harmonic increases.

When the plate vibrates in the secondary branch, its shape changes considerably during the period of vibration, because it is described by a sum of the first and fourth modes and involves both harmonics. Again, the *non-linear* modes of the first and third harmonics are similar - but different - to the linear ones. An example of the plate vibration, for a point in the secondary branch, is shown in Fig. 8. The plots were made at differences of $T/24$, where T represents the period of vibration, and are shown for half a cycle. In the other half of the cycle the plots would be mirror images (symmetric with relation to the plane x-y) of the plots 1 to 12.

As shown in Fig. 9, after $\omega/\omega_{\ell 1} \cong 1.1$ and particularly after $\omega/\omega_{\ell 1} \cong 1.16$, the third harmonic importance in the definition of the first main branch increases significantly, but there is no bifurcation. The first harmonic vibrates in mode 1 - mode (1,1), the second in mode (1,3) - mode 5. Due to a 1:3 internal resonance these modes couple, explaining why the third harmonic is increasingly excited. Both are doubly-symmetric modes. Again, for each maximum amplitude of vibration displacement, the non-linear natural mode shape varies during the cycle of vibration, because it is determined by more than one harmonic.

The mode shapes associated with each harmonic vary with the frequency of vibration, which is equivalent to say that they vary with the maximum amplitude of vibration, due to the effect of the membrane forces. The non-linear mode shape of the plate varies with the maximum amplitude of vibration displacement, because the mode shapes of each harmonic vary and, more significantly, because the relative weight of each harmonic in the definition of the plate's dynamic behavior also changes.

Regarding steady-sate forced vibration, the convergence of the frequency response functions of Plate 3 with the number of harmonics and with the number of out-of-plane and of in-plane shape functions was studied in (Ribeiro and Petyt, 1999d). It was shown that the one harmonic approximation gives remarkably poor results, when the frequency of vibration approaches the first natural frequency and for quite low amplitudes. Accurate results are calculated with two harmonics, and a model with two harmonics will be used in the study of steady-state forced vibrations of Plate 3. In the same reference, it was shown that five out-of-plane shape functions, i.e., 100 d.o.f., provide a precise calculation of the first harmonic and a very good approximation of the third harmonic. Five in-plane shape functions give accurate values for the first harmonic, and the exclusion of the middle plane in-plane displacements (p_i=0) makes the hardening spring effect of both harmonics more severe. The third harmonic is approximately well calculated with five in-plane shape functions, and very accurately calculated with eight in-plane shape functions.

A harmonic excitation at normal incidence with and amplitude given by: $P=2+5\times10^4\ f_2(\xi)\ f_2(\eta)$ N/m^2 was applied to Plate 3. The function f_2 is the second out-of-plane shape function given by

$$f_2 = (1/8)\,\xi - (1/4)\,\xi^3 + (1/8)\,\xi^5 \qquad (41)$$

This excitation has a very similar form to the fourth mode of vibration of the plate.

Figure 10 shows the FRF curves of the first harmonic at $(\xi,\eta)=(0,0)$ and third harmonic at $(\xi,\eta)=(0.5,0.5)$. The first curve has just one peak, which is due to the first mode, mode (1,1). The third harmonic presents a very prominent peak, which is due to excitation of mode 4, mode (2,2). As in free vibration, the fourth mode is excited by means of a 1:3 internal resonance. After this peak, the influence of the fourth mode and the amplitude of vibration decrease. At $W_3/h \cong 0.002$, the FRF curve describes almost a semi-circle. Note that, although the internal resonance occurs at low amplitudes - around W_1/h=0.25 at $(\xi,\eta)=(0, 0)$, it would be disregarded by a harmonic solution.

A normal incident harmonic excitation of large amplitude, 10 N/m^2, was also applied to Plate 3. At large amplitudes it was difficult to achieve convergence, because of the approximated Jacobian used to solve the equations of motion. In order to facilitate convergence, the middle plane in-plane displacements were neglected, which increases the stiffness of the model.

The first harmonic attained a maximum vibration amplitude of around 1.2 times the thickness of the plate and the third harmonic 0.23 – Fig. 11. The shape of the FRF curve at large amplitudes of vibration is different from the typical shape of harmonic solutions, because internal resonance occurs. In fact, at large amplitudes, the vibration of the plate is defined by two non-linear modes: the first - (1,1) - mode, linked with the first harmonic, and the fifth - (1,3) - mode, linked with the third harmonic. The linear natural frequencies of these modes are related by $\omega_{\ell 5}/\omega_{\ell 1} = 3.4712$. When the fifth and the first resonance frequencies become related by $\omega_{n\ell 5}/\omega_{n\ell 1} \cong 3$, there is modal coupling between the first and fifth modes and a 1:3 internal resonance occurs.

The stability of the solutions was studied by solving the eigenvalue problem (38) and three instability areas were detected. The unstable solutions denoted by a circle are of the third order type: they occur in the vicinity of $\omega_{\ell 5}/3$ and stability was lost when a pair of complex conjugate Floquet multipliers crossed the unit cycle. The instability of the solutions denoted by a diamond is probably also of the third order type, as these solutions occur close to $\omega_{\ell 6}/3$. The instability of the solutions denoted by a square is of first order. It was lost with purely real characteristic eigenvalues. Several solutions where modal coupling is present are stable.

Super-harmonic resonance of mode 1 was detected, when the excitation frequency is close to $\omega_{\ell 1}/3$, but its amplitudes of vibration displacement were extremely low.

6 CONCLUSIONS

A model for geometrical non-linear vibration of rectangular plates was developed using the hierarchical finite element method and the harmonic balance method. The equations of motion were solved by a continuation method, with which convergence was achieved even in multi-mode regions and when the solutions are unstable. Symbolic manipulation was employed to accurately integrate high order functions, and define the mass and stiffness matrices and was helpful in the separation of the coefficients of each harmonic.

The convergence with the number of harmonics was studied. The harmonic solution can be very accurate and close to experimental results. However, single harmonic solutions completely ignore modal coupling due to internal resonances, which may occur if the ratio of two linear frequencies is approximately equal to an integer. In free and forced vibration, internal resonances result in multi-frequency, multi-modal vibration and it was shown that stable multi-modal solutions exist. The number of harmonics necessary in the model is limited to the order of internal resonances. In fact, there is no visible difference between the results obtained with two and three odd harmonics when an internal resonance of the type 1:3 occurs.

The excitation of higher order modes due to internal resonance in forced vibration depends on the frequency and spatial form of the excitation applied. On the other hand, the free vibration study allows one to describe all possible internal resonances. Super-harmonic resonances were detected in forced vibration, but, in the absence of internal resonances, their amplitudes of vibration displacement are small.

The convergence of the backbone curves and frequency response functions with the number of shape functions was investigated. The number of out-of-plane displacement shape functions necessary to obtain convergence in non-linear analysis of the isotropic plates studied is approximately the same as in linear analysis of the modes involved. Therefore, the coupling with higher order modes also implies that more d.o.f. are necessary in the spatial model. The middle plane in-plane displacements have a softening spring effect, in the sense that their exclusion makes the stiffness increase more with amplitude. For significant non-linearities, more in-plane shape functions than out-of-plane shape functions are necessary. This is explained by the facts that for each out-of-plane half-wave (visualising the first mode as one half-wave, etc.) two in-plane half-waves exist, and that the importance of the middle plane in-plane displacements increases with the amplitude.

The convergence studies and comparison with published results, demonstrate that the model suggested is characterized by a small number of d.o.f. This results in a very significant economy of time when deriving and solving the equations of motion, and when calculating the characteristic exponents.

The non-linear mode shape changes with the amplitude and frequency of vibration because of two different causes. The first is the variation of the plate's stiffness with the amplitude of vibration and, in this case, the non-linear mode shape maintains a resemblance to the linear one. The second is modal coupling due to internal resonance. In this case, the plate's mode shape changes along the period of vibration.

Waves at grazing and normal incidence were applied, and it was found that more modes are excited when the wave impinges tangentially than normally. The former is a more realistic representation of acoustic excitation and should be preferred in the analysis of aircraft panels.

ACKNOWLEDGMENTS

The second author gratefully acknowledges the scholarship PRAXIS XXI/BD/3868/94 from the *Fundação para a Ciência e a Tecnologia*, Portugal.

REFERENCES

Benamar, R., Bennouna, M. M. K. and White, R. G., 1994, "The effects of large vibration amplitudes on the mode shapes and natural frequencies of thin elastic structures. Part III: fully clamped rectangular isotropic plates-measurements of the mode shape amplitude dependence and the spatial distribution of harmonic distortion", Journal of Sound and Vibration, 175, pp. 377-395.

Chia, C.Y., 1980, Nonlinear Analysis of Plates. New York: McGraw-Hill.

Chiang, C. K., Mei, C. and Gray, C. E., 1991, "Finite element large-amplitude free and forced vibrations of rectangular thin composite plates", ASME Journal of Vibration and Acoustics, 113, pp. 309-315.

Han, W., 1993, The Analysis of Isotropic and Laminated Rectangular Plates Including Geometrical Non-linearity Using the p-version Finite Element Method, Ph.D. Thesis, University of Southampton.

Han, W. and Petyt, M., 1997a, "Geometrically nonlinear vibration analysis of thin, rectangular plates using the hierarchical finite element method - I: The fundamental mode of isotropic plates", Computers and Structures, 63, pp. 295-308.

Han, W. and Petyt, M., 1997b, "Geometrically nonlinear vibration analysis of thin, rectangular plates using the hierarchical finite element method - II: 1st mode of laminated plates and higher modes of isotropic and laminated plates", Computers and Structures 63, pp. 309-318.

Lau, S. L., Cheung, Y. K. and Wu, S. Y., 1984a, "Nonlinear vibration of thin elastic plates. Part 1: Generalised incremental Hamilton's principle and element formulation", ASME Journal of Applied Mechanics, 51, pp. 837-844.

Lau, S. L., Cheung, Y. K. and Wu, S. Y., 1984b, "Nonlinear vibration of thin elastic plates. Part 2: Internal resonance by amplitude-incremental finite element", ASME Journal of Applied Mechanics, 51, 845-851.

Lewandowski, R., 1994, "Non-linear free vibrations of beams by the finite element and continuation methods", Journal of Sound and Vibration, 170, pp. 577-593.

Mei, C. and Decha-Umphai, K., 1985, "A finite element method for non-linear forced vibrations of rectangular plates", AIAA Journal, 23, pp. 1104-1110.

Rao, S. R., Sheikh, A. H. and Mukhopadhyay, M. 1993, "Large-amplitude finite element flexural vibration of plates/stiffened plates", Journal of the Acoustical Society of America, 93, pp. 3250-3257.

Ribeiro, P., 1998, Geometrical Nonlinear Vibration of Beams and Plates by the Hierarchical Finite Element Method, Ph.D. Thesis, University of Southampton.

Ribeiro, P. and Petyt, M., 1999a, "Nonlinear vibration of plates by the hierarchical finite element and continuation methods", International Journal of Mechanical Sciences, 41, pp. 437-459.

Ribeiro, P. and Petyt, M., 1999b, "Nonlinear vibration of composite laminated plates by the hierarchical finite element method", Composite Structures, 46, pp. 197-208.

Ribeiro, P. and Petyt, M., 1999c, "Multi-modal geometrical nonlinear free vibration of composite laminated plates", Journal of Sound and Vibration, 1999, 225, 127-152.

Ribeiro, P. and Petyt, M., 1999d, "Geometrical nonlinear, steady-state, forced, periodic vibration of plates. Part I: Model and convergence studies", Journal of Sound and Vibration, 226, pp. 955-983.

Ribeiro, P. and Petyt, M., 1999e, "Geometrical nonlinear, steady-state, forced, periodic vibration of plates. Part II: Stability study and analysis of multi-modal, multi-frequency response", Journal of Sound and Vibration, 226, pp. 985-1010.

Ribeiro, P. and Petyt, M., 2000, "Nonlinear free vibration of isotropic plates with internal resonance", International Journal of Non-linear Mechanics, 35, pp. 263-278.

Ribeiro, P., 2000, "The second harmonic and the validity of Duffing´s equation for vibration of beams with large displacements", Computers & Structures.

Seydel, R., 1988, From Equilibrium to Chaos. Pratical Bifurcation and Stability Analysis. New York: Elsevier Science.

Szemplinska-Stupnicka, W., 1990, The Behaviour of Non-linear Vibrating Systems. Dordretch: Kluwer Academic Publishers.

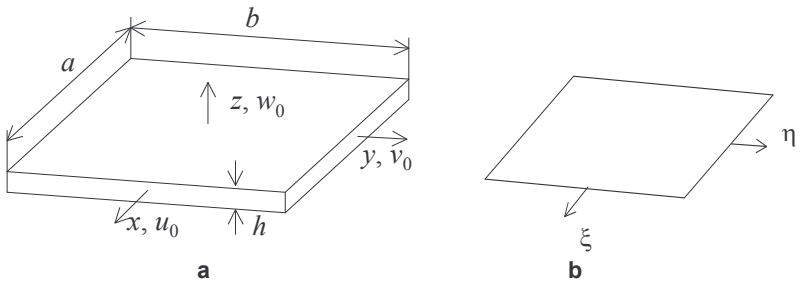

a b

Figure 1. a) Rectangular plate: *x*, *y* and *z* - global coordinate system; u_0, v_0 and w_0 - middle-plane displacements; *a*, *b* and *h* - plate dimensions. b) ξ, η - local coord. system.

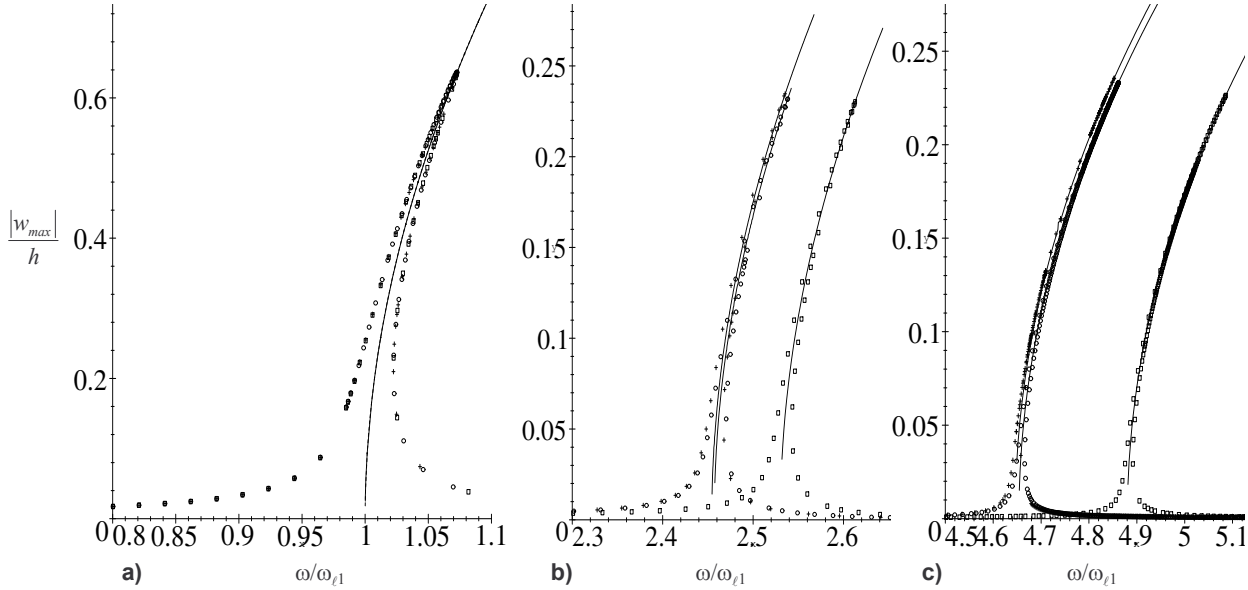

Figure 2. FRFs: □p_o = 2, o p_o = 3, + p_o = 4; Backbone curves: —. Values calculated at (*x*,*y*)=(0,0). a) Mode (1,1), b) mode (1,3), c) mode (1,5).

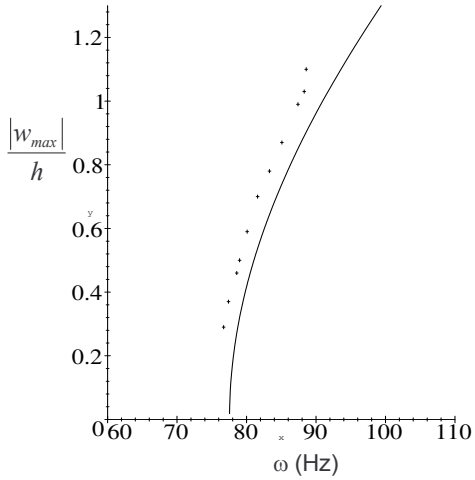

Figure 3. First resonance frequency predicted by the HFEM (p_o = 3 and p_i = 6), —, and measured, +. Plate 1. (*x*,*y*)=(0,0).

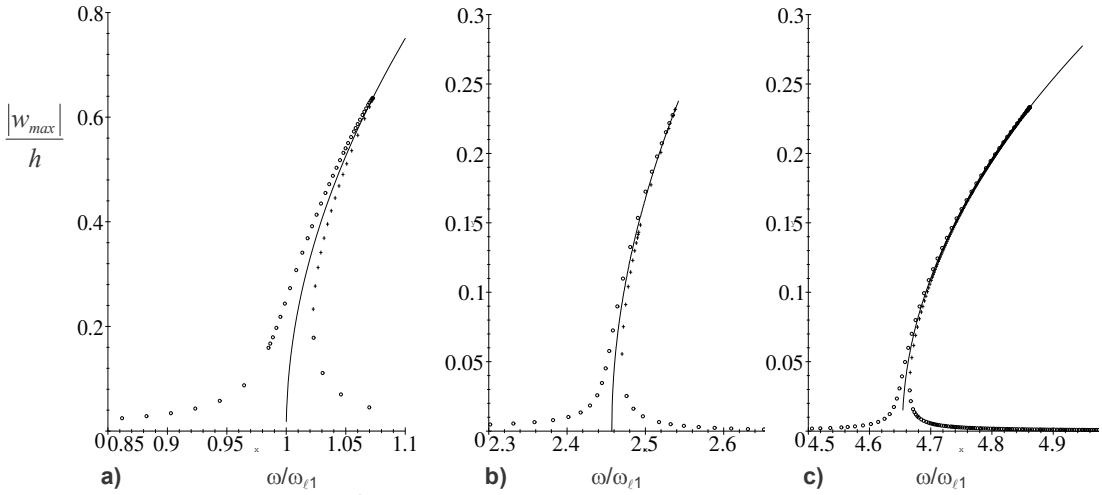

Figure 4. FRF in the vicinity of modes a) (1,1), b) (1,3) and c) (1,5), due to excitation by harmonic plane wave at normal incidence: o stable and + unstable solutions. (*x*,*y*)=(0,0).

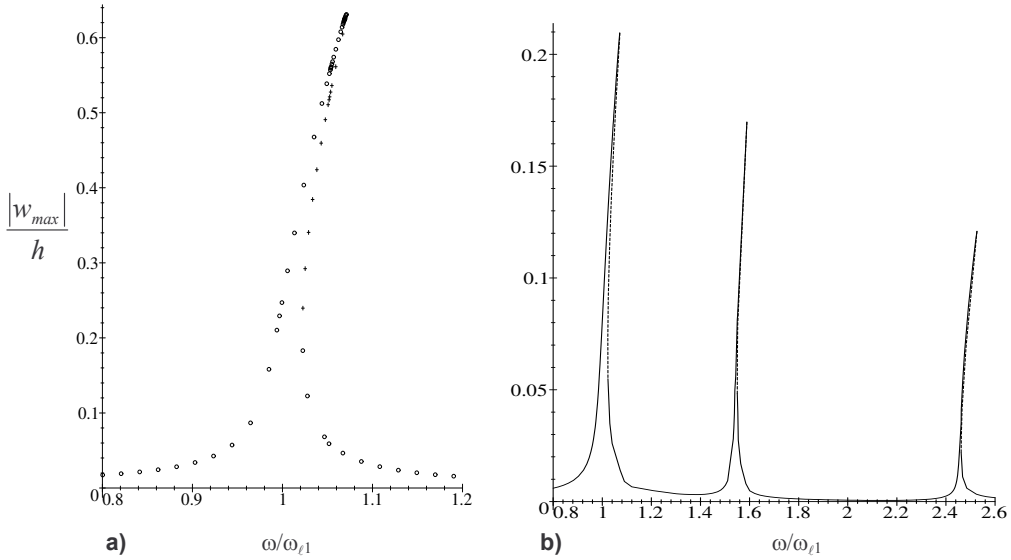

Figure 5. FRF due to excitation by harmonic plane wave at grazing incidence: a) in the vicinity of the first mode at point (*x*, *y*)= (0, 0); b) at point (*x*, *y*)= (*a*/4, *b*/4).

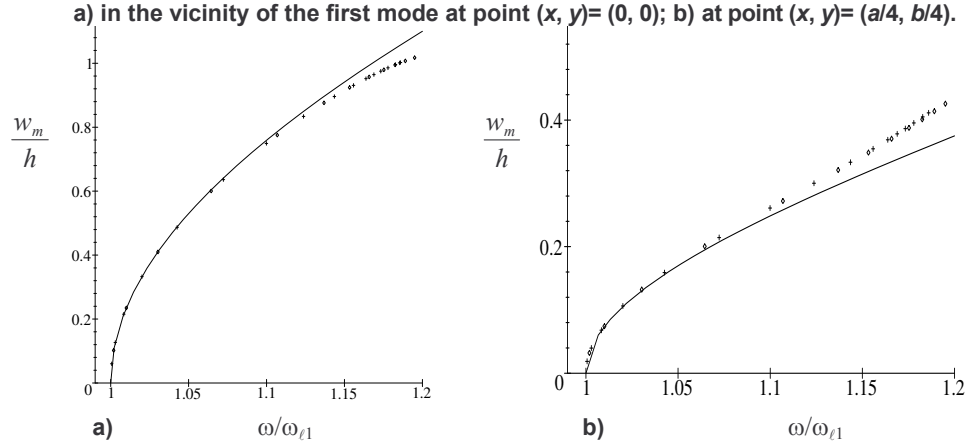

Figure 6. Total amplitude of vibration displacement at a) (ξ,η)=(0,0) and at b) (ξ,η)=(0.5,0.5): - 1 harmonic, ◊ 2 harmonics, + three harmonics (p_o=5, p_i=8).

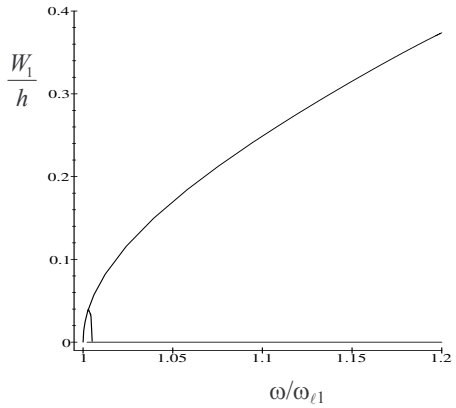

a) From the top: First main branch, secondary branch and second main branch.

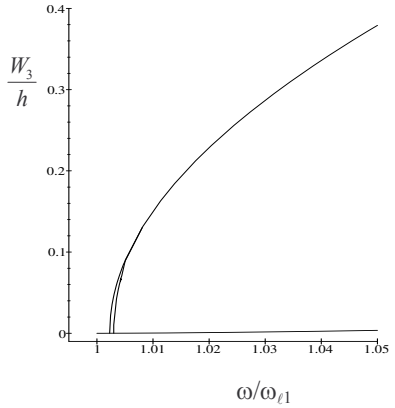

b) From the top: Second main branch, secondary branch and first main branch.

Figure 7. Branch diagrams at (ξ,η)=(0.5,0.5).

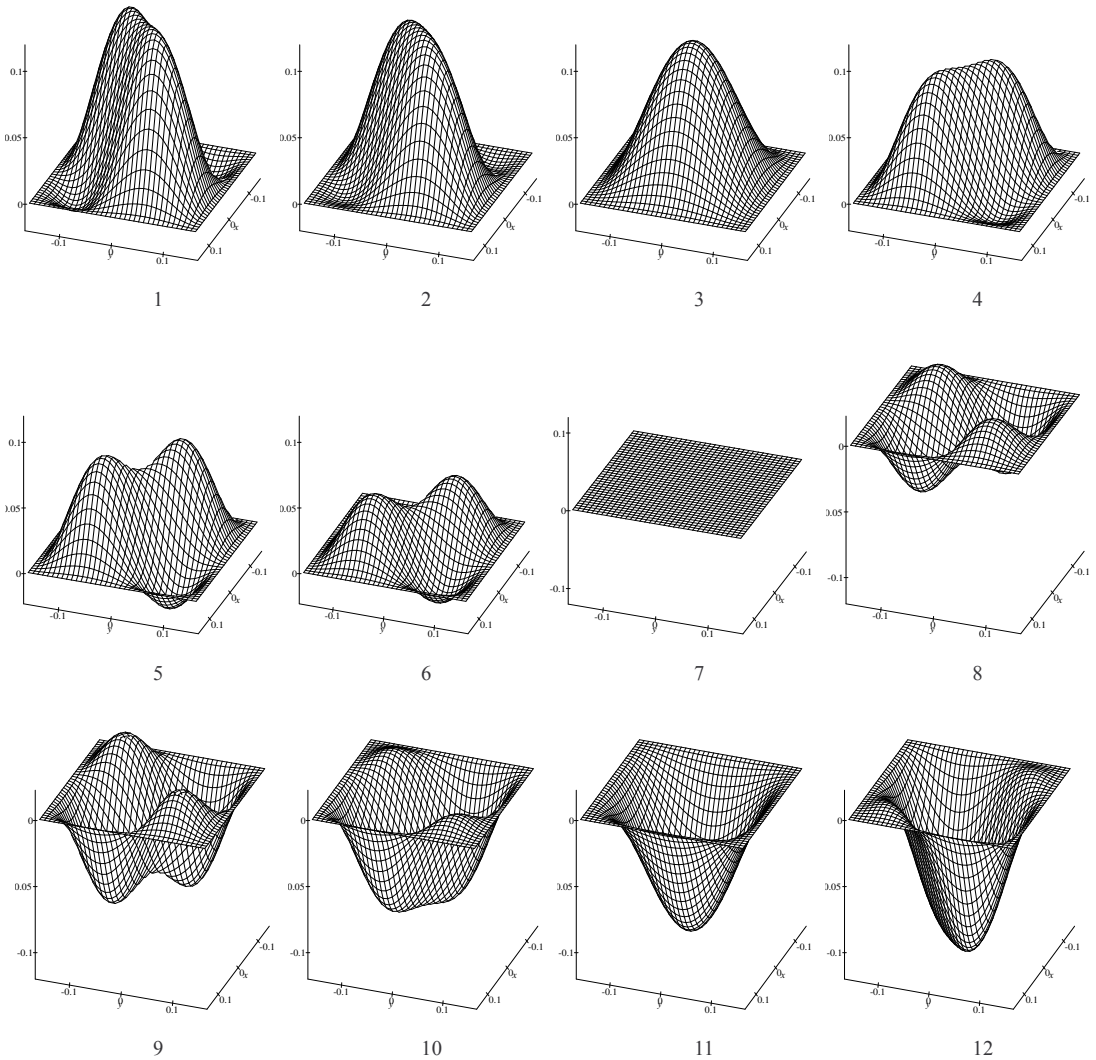

Figure 8. Vibration during half a cycle, at point $\omega/\omega_{\ell 1}$ = 1.0035 of secondary branch.

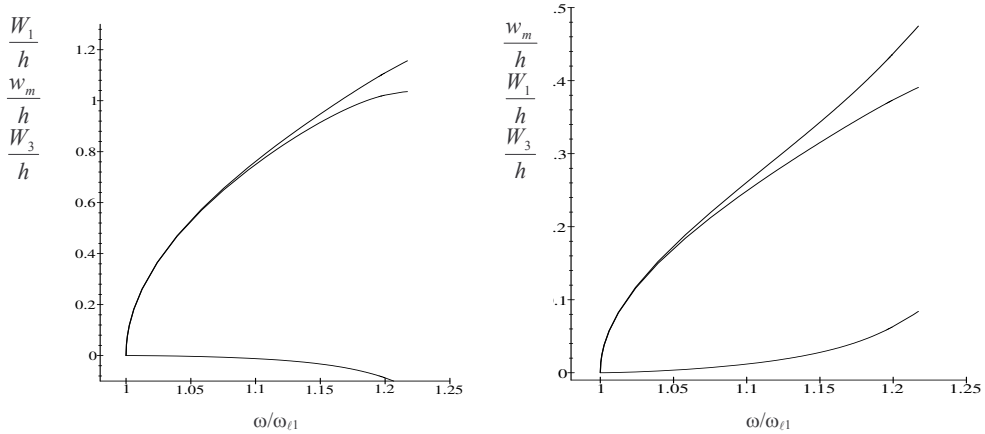

a) (ξ,η)=(0,0). From the top, amplitude of: first harmonic, total, second harmonic.

b) (ξ,η)=(0.5,0.5). From the top: total amplitude, amplitude of first and second harmonics.

Figure 9. First main branch.

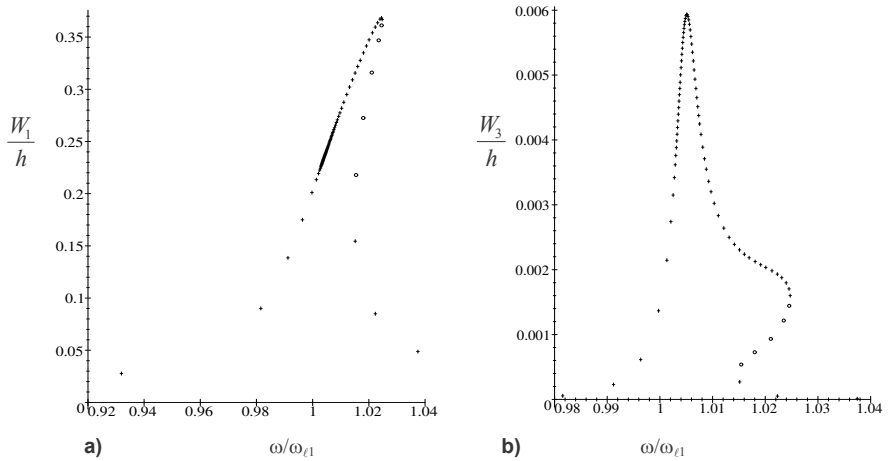

a) b)

Figure 10. FRF of Plate 3 due to non-symmetric excitation: + stable, o unstable. a) First harmonic at (ξ, η) = (0, 0). b) Third harmonic at (ξ, η) = (0.5, 0.5).

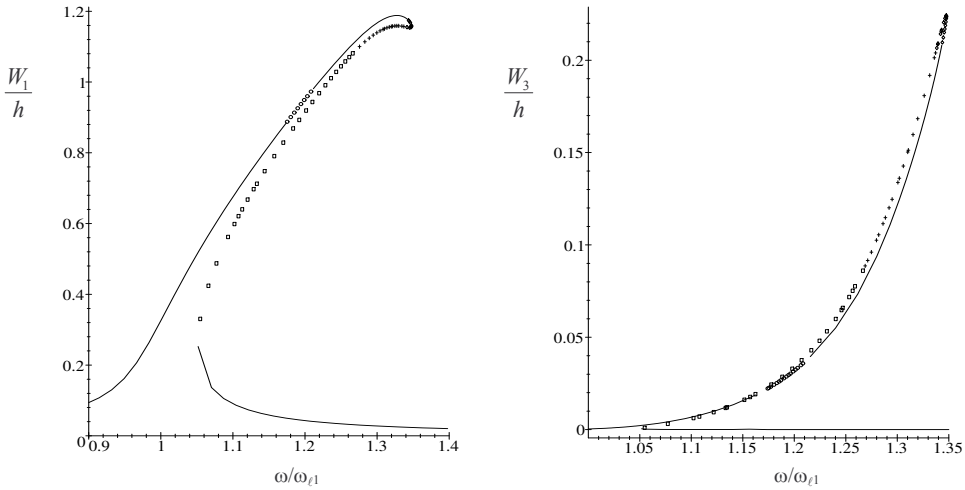

Figure 11. FRF of first and third harmonics at (ξ, η) = (0, 0): – and + stable, o and ◊ third order instabilities, □ first order instability. Plate 3.